ECCOMAS Congress 2016
VII European Congress on Computational Methods in Applied Sciences and Engineering
M. Papadrakakis, V. Papadopoulos, G. Stefanou, V. Plevris (eds.)
Crete Island, Greece, 5–10 June 2016

MIXED SOLID MODELS IN NUMERICAL ANALYSIS OF SLENDER STRUCTURES

D. Magisano[1], **L. Leonetti**[1], **and G. Garcea**[1]

[1]Dipartimento di Infromatica, Modellistica, Elettronica e Sistemistica, Università della Calabria
87030 Rende (Cosenza), Italy
e-mail: domenico.magisano@hotmail.it, leonardo.leonetti@unical.it, giovanni.garcea@unical.it

Keywords: Slender beam and shell, mixed formulations, 3D solid element, Koiter analysis

Abstract. *The reasons of the better performances of mixed, stress–displacements, 3D solid finite elements in the analysis of slender elastic structures are explained. It will be shown that mixed or compatible description, also when derived from the same finite element and then completely equivalent from the discretization point of view, behave very differently when implemented in both asymptotic and path–following solution strategies due to the occurrence of a pathological locking phenomenon in the compatible formulation. The notable advantages of the used of a 3D mixed solid finite element in Koiter asymptotic analysis are also highlighted.*

1 INTRODUCTION

In recent years an increasing amount of research has aimed at developing new efficient solid finite elements [1] for the linear and nonlinear analysis of thin structures. This is due to the advantages of solid elements in comparison to classical shell elements. In particular in the elastic nonlinear analysis of slender structures they allow the use of the 3D continuum strain and stress measures employing translational degrees of freedom only [1, 2, 3, 4]. In this way it is possible to avoid the use of complicated and expensive rules for updating the rotations and, by using the Green-Lagrange strain measure, to coherently describe the structural behavior through a low order dependence on the displacement field. Moreover in this context, solid elements allow: a simpler expression of the strain energy and its variations with a gain in computational efficiency; the recovery of the complete 3D stress state and the application of nonlinear constitutive laws; simpler geometric and kinetic descriptions; the simple discretization of structures with both solid and shell-like regions. Furthermore the independence of the model from rigid body motion or change in the observer (objectivity) is automatically fulfilled without the need to employ complex, geometrically exact formulations, which are not always available or accurate [5, 6, 7].

However, formulating robust solid-shell elements is more demanding than shell elements. To maintain an acceptable number of degrees of freedom, the elements proposed are usually based on a low order displacement interpolation. Consequently they have the disadvantages of *interpolation lockings*: the shear and membrane locking also present in classical shell elements and trapezoidal and thickness locking, typical of low order solid-shell elements [8]. Interpolation lockings are usually sanitized by means of Assumed Natural Strain, Enhanced Assumed Strain [9, 10, 11, 12] and mixed (hybrid) formulations [1, 4, 13, 14]. In this way solid-shell elements have now reached a high level of efficiency and accuracy and have also been used to model composites or laminated beams [11, 15, 13, 16] and shell structures in both the linear [9, 3] and nonlinear [12, 2, 1] range. Among the most effective and interesting proposals we refer to are the mixed solid-shell elements of Sze and coauthors [1, 13, 17, 18, 19, 20, 21, 16, 22, 23] which extend the initial PT18β hybrid element of Pian and Tong to thin shell.

When comparing mixed and compatible finite elements many authors (see for example [1] and [2]) observe that the mixed ones are more robust and allow larger steps in path–following geometrically nonlinear analyses. However the reasons for these better performances are, in our opinion, not clear, as they are often wrongly attributed to the properties of the finite element interpolation. One of the goals of this paper is therefore to clarify the true reason and the origin of this phenomenon, extending the results presented some years ago [24, 25] in the context of path-following and Koiter [26, 27, 28] asymptotic analyses of 2D framed structures.

Mixed and compatible description, while completely equivalent at the continumm level, behave very differently when implemented in path-following and asymptotic solution strategies even when they are based on the same finite element interpolations, that is when they are equivalent also at the discrete level. This is an important, even if frequently misunderstood, point in developing numerical algorithms and it has been discussed in [24, 25, 29] to which we refer readers for more details. To represent the strain energy in a *smooth enough* way in order to make the truncation error of its Taylor expansion up to a given order as small as possible is crucial: in path-following analysis, this ensures a fast convergence of the Newton (Riks) iterative process; in asymptotic analysis, which is based on Taylor series the expansion of the strain energy [26, 28] implies an accurate recovery of the equilibrium path. Since the smoothness of a nonlinear function strictly depends on the set of variables used for its description, a key point to

be considered when approaching the solution of a nonlinear problem is the selection of the most appropriate set of variables. In fact mixed and compatible descriptions are characterized by a different smoothness of the strain energy and so they behave very differently when used within a numerical solution process. In particular representing the strain energy by using displacements only (compatible description) as variables has to be considered the least suitable choice as, in this case the truncation error of a Taylor expansion depends, pathologically, on the presence of directions with very different stiffness, while this is not the case in a mixed format. For shells or beams, in the presence of large displacements (rigid rotations) and high membranal/flexural stiffness ratios, the truncation error of the compatible description becomes large and causes a very slow convergence rate in path-following analysis and an unreliable estimate of the bifurcation point and of the post–critical coefficients in the asymptotic analysis. As will be shown, using solid elements means the mixed description is unaffected by this kind of locking, that we call *extrapolation locking*.

In this paper a mixed and a compatible description are derived for the same finite element, so obtaining two completely equivalent discrete problems, in order to show that their different behavior is not due to the interpolation fields and that the extrapolation locking occurs for any compatible finite element. This is an important aspect not taken into account by the scientific community because, usually, lockings are attributed to the interpolation only.

Moreover, note that the solid element based on the quadratic Green-Lagrange strain measure, minimizes the strain energy dependence on the finite element (FE) discrete variables: the fourth order dependence on displacement variables in the compatible formulation and the third order in stress and displacement variables in the mixed case. Although this does not produce any real important benefit with respect to the extrapolation locking it does however have a significant effect on the efficiency, robustness and coherence of the asymptotic analysis when the mixed description is used. It allows, in fact, the zeroing of all the strain energy variations of an order greater than the third and, consequently, permits light numerical formulations and an improvement in accuracy. In this way it is possible to develop new asymptotic algorithms well suited to the imperfection sensitivity analysis of structures presenting coincident or almost coincident buckling loads, which are more accurate and computationally efficient than those based on classical shell elements. This advantage holds in standard path-following analysis where however it only allows simpler expressions of the tangent stiffness matrix and the structural response.

Finally it is worth mentioning that the use of both displacement and stress variables increases the dimension of the problem, but generally the computational extra–cost, with respect to a compatible analysis, is very low. This is because the global operations involve displacement dofs by performing a static condensation of the stress variables, when locally defined at element level. This small computational extra-cost is largely compensated for: in path-following analysis by larger steps and fewer iterations with respect to the compatible case; in asymptotic analysis by the zeroing of the computationally expensive fourth order strain energy variations. We will also show how the small nonlinearity that the equilibrium path assumes when represented in mixed variables allows, in path following analyses, an efficient use of the modified Newton method with a further significant reduction in the computational cost.

2 MIXED AND COMPATIBLE DESCRIPTIONS

In this section, two equivalent descriptions, one in stresses and displacements called *mixed description* and another in displacement parameters only, called *compatible description*, are derived. We refer to [29, 28, 7, 6] for a description of the asymptotic method.

2.1 The discrete nonlinear equations

We consider a slender hyperelastic structure subject to conservative loads $p[\lambda]$ proportionally increasing with the amplifier factor λ. The equilibrium is expressed by the virtual work equation

$$\Phi[u]'\,\delta u - \lambda \hat{p}\,\delta u = 0 \quad , \quad u \in \mathcal{U}\ ,\ \delta u \in \mathcal{T} \tag{1}$$

where $u \in \mathcal{U}$ is the field of configuration variables, $\Phi[u]$ denotes the strain energy, $\mathcal{T}$ is the tangent space of $\mathcal{U}$ at u and a prime is used to express the Frechèt derivative with respect to u. We assume that $\mathcal{U}$ will be a linear manifold so that its tangent space $\mathcal{T}$ will be independent of u. When a mixed format is adopted the configuration variables u collect both displacement and stress fields.

The element strain energy can, as usual in a FE context, be expressed as a sum of element contributions that, using a mixed interpolation for the displacement and the stress field $\boldsymbol{\sigma}$ and letting with Ω_e the element domain, becomes

$$\begin{aligned}
\Phi[u] &\equiv \sum_e \Phi_e[u] = \sum_e \int_{\Omega_e} \left(\boldsymbol{\sigma}^T \boldsymbol{\varepsilon} - \frac{1}{2}\boldsymbol{\sigma}^T \mathbf{C}^{-1} \boldsymbol{\sigma} \right) dV_e \\
&= \boldsymbol{\beta}^T (\mathbf{L} + \frac{1}{2}\mathbf{Q}[\mathbf{d}])\mathbf{d} - \frac{1}{2}\boldsymbol{\beta}^T \mathbf{H} \boldsymbol{\beta} \\
\Phi_e[u] &= \boldsymbol{\beta}_e^T (\mathbf{L}_e + \frac{1}{2}\mathbf{Q}_e[\mathbf{d}_e])\mathbf{d}_e - \frac{1}{2}\boldsymbol{\beta}_e^T \mathbf{H}_e \boldsymbol{\beta}_e
\end{aligned} \tag{2}$$

where $\boldsymbol{\varepsilon}$ is the Green-Lagrange strain measure $\mathbf{L}$ and $\mathbf{Q}[\mathbf{d}]$ are the linear and quadratic discrete compatibility matrices, $\mathbf{d}$ is the vector collecting all the finite element displacement variables while $\boldsymbol{\beta}$ is the vector collecting all the stress parameters, $\mathbf{C}$ and $\mathbf{H}$ are the continuum and discrete elastic matrices and a subscript 'e' denotes the corresponding finite element quantities. It is worth to note as, by using the Green strain measure, the mixed strain energy (2) has a third order nonlinearity with respect to the configuration variable vector $\mathbf{u} = \{\boldsymbol{\beta}, \mathbf{d}\}$.

The element can also be described in a compatible format by requiring that the discrete form of the constitutive laws is "a priori" satisfied. As in the present FE model the stress variables are locally defined at the element level we have

$$\boldsymbol{\beta}_e[\mathbf{d}_e] = \mathbf{H}_e^{-1}(\mathbf{L}_e + \frac{1}{2}\mathbf{Q}_e[\mathbf{d}_e])\mathbf{d}_e \tag{3}$$

where, to highlight that in the compatible format the stresses are not independent variables, we explicitly report the dependence of $\mathbf{d}_e$.

Substituting Eq.(3) in Eq.(2) we obtain the *compatible description* of the element strain energy

$$\Phi_e = \frac{1}{2}\left\{ \mathbf{d}_e^T (\mathbf{L}_e + \frac{1}{2}\mathbf{Q}_e[\mathbf{d}_e])^T \mathbf{H}_e^{-1} (\mathbf{L}_e + \frac{1}{2}\mathbf{Q}_e[\mathbf{d}_e])\mathbf{d}_e \right\} \tag{4}$$

that has a 4th order dependence on the displacement variables only.

Similarly a fourth order dependence of the strain energy from the displacements parameters, is obtained with any compatible finite element interpolation when a 3D solid formulation is employed. In this paper we intentionally use the compatible description derived from the mixed finite element in order to have the same discrete approximation for both the description, i.e. the finite element is the same but the format of the problem changes. This allows us to focus of the way as the problem description affects its solution in large deformation problems (see

also [24, 25]) and then to show the reasons of the better performance of the use of a mixed description. The conclusions are general and hold for any other compatible or mixed finite element. In the numerical experiments the Pian and Tong PT18 element [50] will be used.

2.2 Tangent stiffness matrix for mixed and compatible descriptions

Eq.(2) allows the expression of the strain energy as an algebraic nonlinear function of the element vector

$$\mathbf{u}_e := \begin{bmatrix} \boldsymbol{\beta}_e \\ \mathbf{d}_e \end{bmatrix} \tag{5}$$

related to the vector $\mathbf{u}$, collecting all the parameters of the FE assemblage, through the relation

$$\mathbf{u}_e = \boldsymbol{\mathcal{A}}_e \mathbf{u} \tag{6}$$

where matrix $\boldsymbol{\mathcal{A}}_e$ contains the link between the elements. Furthermore we denote with $\delta\mathbf{u}_{ei} = \{\delta\boldsymbol{\beta}_{ei}, \delta\mathbf{d}_{ei}\}$ the element vector corresponding to the variation $\delta\mathbf{u}_i$.

Exploiting the linear dependence of $\mathbf{Q}_e[\mathbf{d}_e]$ from $\mathbf{d}_e$ and its symmetry we have

$$\begin{aligned} \mathbf{Q}_e[\mathbf{d}_{e1}]\mathbf{d}_{e2} &= \mathbf{Q}_e[\mathbf{d}_{e2}]\mathbf{d}_{e1}, \quad \forall \mathbf{d}_{e1}, \mathbf{d}_{e2} \\ \boldsymbol{\beta}_e^T \mathbf{Q}_e[\mathbf{d}_e]\mathbf{d}_e &= \mathbf{d}_e^T \boldsymbol{\Gamma}_e[\boldsymbol{\beta}_e]\mathbf{d}_e \end{aligned} \tag{7}$$

and the second strain energy variation on the mixed element is obtained as

$$\begin{aligned} \Phi_e'' \delta u_1 \delta u_2 &= \begin{bmatrix} \delta\boldsymbol{\beta}_{e1} \\ \delta\mathbf{d}_{e1} \end{bmatrix}^T \begin{bmatrix} -\mathbf{H}_e & \mathbf{B}_e[\mathbf{d}_e] \\ \mathbf{B}_e[\mathbf{d}_e]^T & \boldsymbol{\Gamma}_e[\boldsymbol{\beta}_e] \end{bmatrix} \begin{bmatrix} \delta\boldsymbol{\beta}_{e2} \\ \delta\mathbf{d}_{e2} \end{bmatrix} \\ &= \delta\mathbf{u}_{e1}^T (\mathbf{K}_{0e} + \mathbf{K}_{1e}[\mathbf{u}_e]) \delta\mathbf{u}_{e2} \end{aligned} \tag{8}$$

where δu_i are generic variations of the configuration field u and $\delta\mathbf{u}_i$ the corresponding FE vectors. Eq.(8) provides the element tangent stiffness matrix $\mathbf{K}_e[\mathbf{u}_e] = \mathbf{K}_{0e} + \mathbf{K}_{1e}[\mathbf{u}_e]$ as a sum of the linear elastic contribution $\mathbf{K}_{0e}$ and the geometric matrix $\mathbf{K}_{1e}[\mathbf{u}_e]$ implicitly defined in Eq.(8).

For the compatible description we have

$$\Phi_e'' \delta u_1 \delta u_2 = \delta\mathbf{d}_{e1}^T \left\{ \mathbf{B}_e^T[\mathbf{d}_e] \mathbf{H}_e^{-1} \mathbf{B}_e[\mathbf{d}_e] + \boldsymbol{\Gamma}[\boldsymbol{\beta}_e[\mathbf{d}_e]] \right\} \delta\mathbf{d}_{e2} \tag{9}$$

where the tangent stiffness matrix has a second order dependence on $\mathbf{d}_e$. To emphasize this we write

$$\mathbf{K}_e = \mathbf{K}_{0e} + \mathbf{K}_{1e}[\mathbf{d}_e] + \mathbf{K}_{2e}[\mathbf{d}_e, \mathbf{d}_e] \tag{10}$$

Finally the evaluation the whole matrix is obtained by standard asseblage as

$$\mathbf{K} = \sum_e \boldsymbol{\mathcal{A}}_e^T \mathbf{K}_e \boldsymbol{\mathcal{A}}_e. \tag{11}$$

2.3 Advantages of mixed solid finite elements in path-following and asymptotic analysis of slender structures

FE models directly derived from the 3D continuum using the Green strain measure have a low order dependence on the strain energy from the discrete FE parameters: $3rd$ and $4th$ order for mixed and compatible respectively. On the contrary geometrically exact shell and beam models [5, 6] or those based on corotational approaches [26, 47, 51], explicitly make use of

the rotation tensor and its highly nonlinear representation. This implies that the strain energy is infinitely differentiable with respect to its parameters and leads to very complex expressions for the energy variations with a high computational burden of path following and much more of asymptotic analyses. In this last case the high order strain energy variations become so complex that often "ad hoc" assumptions are required to make the solution process effective (see section 4.3 of [26]). The consequence is that the fewer global degrees of freedom that could be employed using a shell FE model do not necessarily imply a lesser computational cost as it depends, from the others, on the cost of evaluation of the strain energy variations. On the contrary for solid finite elements the strain energy, in both compatible and mixed form, has the lowest polynomial dependence on the corresponding discrete parameters and in particular in the mixed format of Eq.(2) has just one order more than in the linear elastic case. It implies the zeroing of all the fourth order strain energy variations required by the Koiter analysis with important advantages in terms of both computations and coherence of the method.

3 THE EXTRAPOLATION LOCKING AND ITS CURE USING MIXED SOLID ELEMENT

In this section the better performances of the mixed description in geometrically nonlinear analysis, in terms of robustness, efficiency and, relative to Koiter formulation, also in terms of accuracy, are shown and explained. In this context the compatible description of the problem, whatever the FE and the structural model used, is affected by a pathological *extrapolation locking* phenomenon investigated for the first time for 2D frames in [24, 25].

3.1 Mixed versus compatible description in path-following analysis

The convergence of the Riks scheme is as fast as the iteration stiffness matrix $\tilde{\mathbf{K}}$ is near to $\mathbf{K}_s$ and then, as slow $\mathbf{K}[\mathbf{u}]$ changes with $\mathbf{u}$. The similarity of the stiffness matrices in two different points $\mathbf{K}_j \equiv \mathbf{K}[\mathbf{u}_j]$ and $\mathbf{K}_{j+1} \equiv \mathbf{K}[\mathbf{u}_{j+1}]$ is evaluated by the difference (see [24])

$$\Delta k[\mathbf{u}] \equiv \mathbf{u}^T(\mathbf{K}_{j+1} - \mathbf{K}_j)\mathbf{u} = \Phi''_{j+1}u^2 - \Phi''_j u^2 \tag{12}$$

For the mixed description we have

$$\Delta k_M[\mathbf{u}] = \Phi'''_j(u_j - u_i)u^2 = \mathbf{d}^T\boldsymbol{\Gamma}[\boldsymbol{\beta}_{j+1} - \boldsymbol{\beta}_j]\mathbf{d} + 2\boldsymbol{\beta}^T\mathbf{Q}[\mathbf{d}](\mathbf{d}_{j+1} - \mathbf{d}_j) \tag{13}$$

while for the compatible description the same quantity becomes

$$\begin{aligned}\Delta k_C[\mathbf{u}] &= \Phi'''_j(u_j - u_i)u^2 + \frac{1}{2}\Phi''''_j(u_j - u_i)^2u^2 \\ &= \mathbf{q}_{j+1}^T\mathbf{H}^{-1}\mathbf{q}_{j+1} - \mathbf{q}_j^T\mathbf{H}^{-1}\mathbf{q}_j + \mathbf{d}^T(\boldsymbol{\Gamma}[\boldsymbol{\beta}[\mathbf{d}_{j+1}] - \boldsymbol{\beta}[\mathbf{d}_j]])\mathbf{d}\end{aligned} \tag{14}$$

where $\mathbf{q}_{j+1} = \mathbf{B}[\mathbf{d}_{j+1}]\mathbf{d}$ and $\mathbf{q}_j = \mathbf{B}[\mathbf{d}_j]\mathbf{d}$.

For slender structures it occurs that $\boldsymbol{\beta}_{j+1} \approx \boldsymbol{\beta}_j$ undergoing large rigid element deformations and very small stress and strain increments and then

$$\Delta k_M \approx 2\boldsymbol{\beta}^T(\mathbf{q}_{j+1} - \mathbf{q}_j) \tag{15}$$

and

$$\Delta k_C \approx f[\mathbf{q}_{j+1}] - f[\mathbf{q}_j] \quad \text{with} \quad f[\mathbf{q}] = \mathbf{q}^T\mathbf{H}^{-1}\mathbf{q} \tag{16}$$

When, as is usual for slender structures, the condition number of $\mathbf{H}$ is high due to very different stiffness ratios (i.e. membranal/flexural) the ellipsoids associated to $\mathbf{H}$

$$\mathcal{E} \equiv \{\mathbf{q} : \mathbf{q}^T\mathbf{H}\mathbf{q} = 1\}$$

are very stretched. As $f[\mathbf{q}]$ is related to the radius $r[\mathbf{q}]$ of $\mathcal{E}$ in the direction $\mathbf{q}$ by the following expression

$$f[\mathbf{q}] = r[\mathbf{q}]^2(\mathbf{q}^T\mathbf{q})$$

Δk_c becomes

$$\Delta k_C \approx r^2[\mathbf{q}_{j+1}]\mathbf{q}_{j+1}^T\mathbf{q}_{j+1} - r^2[\mathbf{q}_j]\mathbf{q}_j^T\mathbf{q}_j$$

In this case even small differences in the direction of $\mathbf{q}_{j+1}$ and $\mathbf{q}_j$ may produce a large Δk_C growing with the condition number of $\mathbf{H}$ even when the Euclidean norm of the two vectors is similar (see Fig.1). This produces, in path following analyses a pathological reduction in the

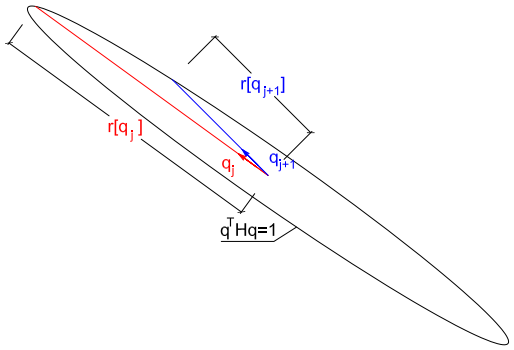

Figure 1: Graphical interpretation of Δk for the compatible description

step length, an increase in the total number of the iterations and, sometimes, the loss of convergence. This phenomenon is called *extrapolation locking* from which the mixed models are free because they are unaffected by the "hard terms" in $\mathbf{H}^{-1}$ and Δk_M is proportional to the difference $\mathbf{q}_{j+1} - \mathbf{q}_j$. As expressions like those in Eqs.(13) and (14) are obtainable using any mixed or compatible finite element the conclusions reported here can be generalized. In particular note that for any structural model the strain energy can be expressed as a quadratic function of the stress variables through the Hellinger-Reissner principle and so its higher order variations are not influenced by $\mathbf{H}$. On the contrary all the compatible strain energy variations always involve terms in $\mathbf{H}^{-1}$. This means that extrapolation locking heavily affects any compatible finite element/description while it does not occur in mixed formulation.

We show the occurrence of the locking in the simple case of the Euler beam, for which the geometry and load conditions are reported in fig. 2.

In tab.2 the number of steps and iterations (loops) to obtain the equilibrium path, directly related to the CPU time, are presented. The results of the mixed formulation, denoted by M, are unaffected by the coefficient $k = (t/\ell)^2$ while the compatible ones (C) pathologically depend on it.

Finally in Fig.3 we report the minimum ρ_{min} and maximum ρ_{max} absolute value of the eigenvalues of the matrix $\mathbf{K}_{n+1}\mathbf{K}_n^{-1}$ for both descriptions, where $n+1$ and n denote two equilibrium points. The set of points in which the ρs are evaluated belongs on the equilibrium path obtained by the mixed description. It is important to observe how the mixed description ρ_{max} is independent of k and has almost the optimal value 1.0 while for the compatible description it

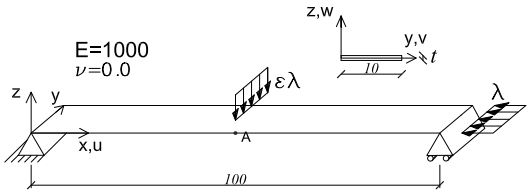

	Compatible				Mixed
k	10^4	10^5	10^6	10^7	(all k)
steps	38	43	67	failed	27
loops	133	166	328	failed	75

Figure 2: Eulero beam: analysis evolution for increasing k, mesh $1 \times 1 \times 40$

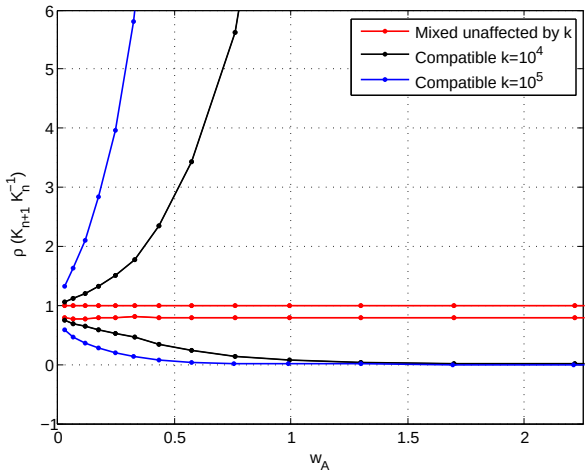

Figure 3: Minimum and maximum eigenvalues of matrix $\mathbf{K}_{n+1}\mathbf{K}_n^{-1}$ for the simple tests

increases with the step length. Also note that is the extrapolation locking that heavily affects also the convergence of the arc-length solution while the singular direction is filtered by the Riks constraint. We refer readers to [24, 25] for further details.

3.2 Mixed vs compatible description in Koiter analysis using 3D solid elements

As the Koiter method is based on Taylor expansion of the strain energy the use of a mixed description has a tremendous impact not only in terms of efficiency but also of accuracy. For any finite element (see [25, 35, 6]) the mixed description makes the truncation independent of $\mathbf{H}^{-1}$ and small with respect to the retained terms.

Using compatible format in Koiter analysis the locking already occurs in the evaluation of the buckling loads (see [25]). To avoid extrapolation locking usually the compatible bifurcation analysis is performed by zeroing the quadratic displacements terms into the tangent stiffness matrix (*direct extrapolation* hypothesis) or by evaluating the geometric terms using zeroed displacements (*frozen configuration* hypothesis). In both cases the bifurcation search reduces to a linear eigenvalue problem.

In Tab.1 the buckling loads obtained from the various descriptions and locking cures are presented for the Euler beam of Fig. 2 by changing both the aspect ratio k and the imperfection load amplitude ϵ. In particular we denote with (C) and (M) the results obtained respectively with the compatible and mixed description and by (F) and (D) those of the frozen configuration and direct extrapolation respectively. For this case which has small precritical nonlinearities it is worth noting that: i) the frozen configuration hyphothesis sanitizes the locking effect and fur-

Table 1: Bifurcation locking for the Euler beam/(exact value for the elastica)

k	$\epsilon = 0.01$		$\epsilon = 0.005$		$\epsilon = 0.001$		for all ϵ	
	C	D	C	D	C	D	F	M
10^4	failed	0.673	1.112	0.865	1.004	0.994	1.001	1.001
10^5	failed	0.309	failed	0.517	1.040	0.937	1.001	1.001
10^6	failed	0.111	failed	0.209	failed	0.673	1.001	1.001
10^7	failed	0.033	failed	0.071	failed	0.308	0.999	0.999

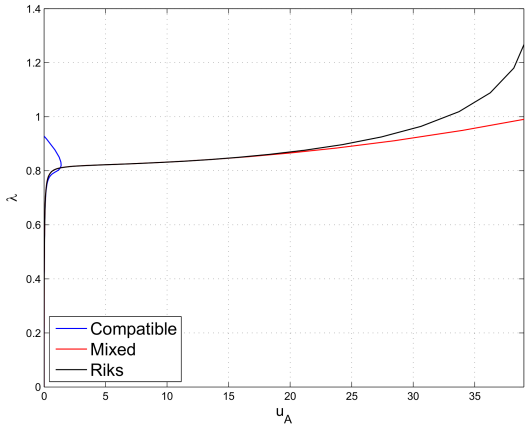

Figure 4: Equilibrium path for the Euler beam for $\epsilon = 0.001$ and $k = 10^4$

nishes accurate results; ii) the compatible description misses the bifurcation point and the direct extrapolation furnishes an inaccurate solution, getting worse with the precritical nonlinearity due to the transversal force. Inaccuracy on the bifurcation points obviously leads to completely wrong equilibrium path evaluation.

The zeroing of all the precritical displacements could, however, lead to inaccuracy when the precritical displacements are not negligible as in the shallow arc reported in Fig.5. In this case the frozen configuration is not capable of producing the correct bifurcation load and mode as reported in Tab.2. The buckling point is used to evaluate the energy terms also reported in Tab.2, so the equilibrium path obtained with the frozen configuration hyphothesis is very inaccurate. In Fig.6 the equilibrium path of the Koiter mixed formulation is presented and compared with the frozen one and path following solution.

However the great advantage in adopting mixed solid elements in Koiter analysis is in the evaluation of all the fourth order coefficients required by the formulation (see [29]) that, for mixed solid elements, requires only second variations for their evaluation since the usually very complex fourth order strain energy variations are automatically zero.

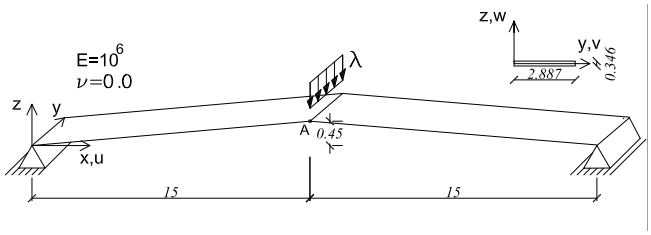

Figure 5: Geometry and material properties of the shallow arc

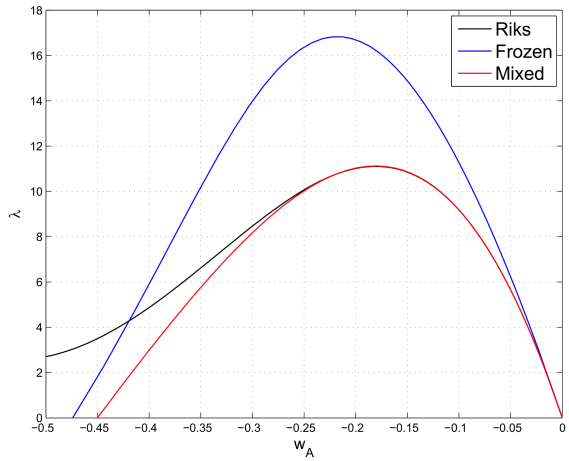

Figure 6: Equilibrium path for the shallow arc

	M	*F*
λ_1	22.0202	30.6526
λ_2	30.6671	47.0652
$\mathcal{A}_{001}$	0.0196	0.0190
$\mathcal{A}_{111}$	47.9305	182.3644
$\mathcal{B}_{0011}$	-6.32 10^{-4}	0
$\mathcal{B}_{1111}$	8.2117	207.3178

Table 2: Shallow arc: comparison of relevant energy asymptotic quantities

	Mixed	Frozen
λ_1	1266.8	1291.5
λ_2	1828.1	1719.0
λ_3	3092.3	2949.7
λ_4	3114.7	2970.6

Table 3: Channel section: first 4 buckling loads.

4 NUMERICAL RESULTS

In this section the effectiveness and reliability of both methods of analysis are tested in a series of benchmark problems. In particular for the path-following analysis the efficiency of the mixed description, which allows very large steps in comparison with the compatible one, is highlighted. For the asymptotic formulation we show the accuracy given by the mixed solid element.

For all the tests only one element in the thickness is used while the same convergence conditions and arc-length parameters are adopted for mixed and compatible path-following analyses. The label Riks denotes the equilibrium paths obtained by the arc-length scheme (the same for both the description), while labels Mixed and Frozen denote the asymptotic paths using mixed and compatible frozen descriptions.

4.1 Simply supported C-shaped beam

The first test, with geometry and material reported in figure 7, consists in a simply supported compressed beam with a C shaped section. It presents a nonlinear prebuckling behavior due to two forces (torsional imperfections) at the mid-span and coupled instability. For this reason it is a good benchmark to test the accuracy of the asymptotic analysis. A similar test was studied

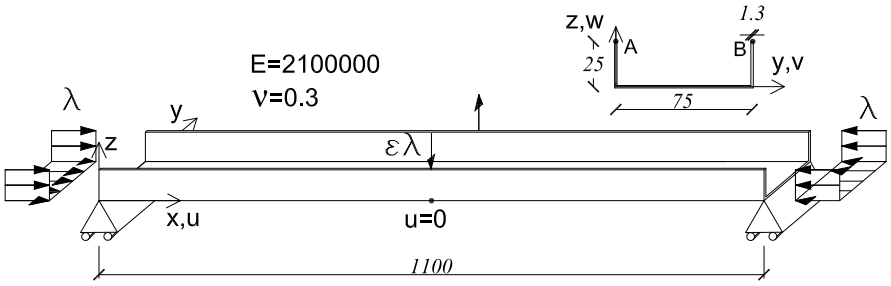

Figure 7: Channel section: geometry and loads.

in [35] using shell elements and in [52] using a generalized beam model. The buckling values, obtained by using a mesh of $(8+8+18)\times 50$ elements are reported in Table 3 and compared with those computed using the compatible description with the frozen configuration hyphothesis. The Koiter analysis uses the first four buckling modes plotted in Fig.8. It is possible to see how the first two modes are global, essentially flexural and torsional respectively, while the others are local modes.

The accuracy of the mixed asymptotic strategy in the evaluation of the limit load and of the initial postcritical behavior is shown in Fig.9. It is also possible to observe the poor accuracy of the frozen configuration analysis in estimating both the limit load and equilibrium path. In Fig.10 the equilibrium path of Koiter method, in terms of the modal contributions ξ_k, is plotted.

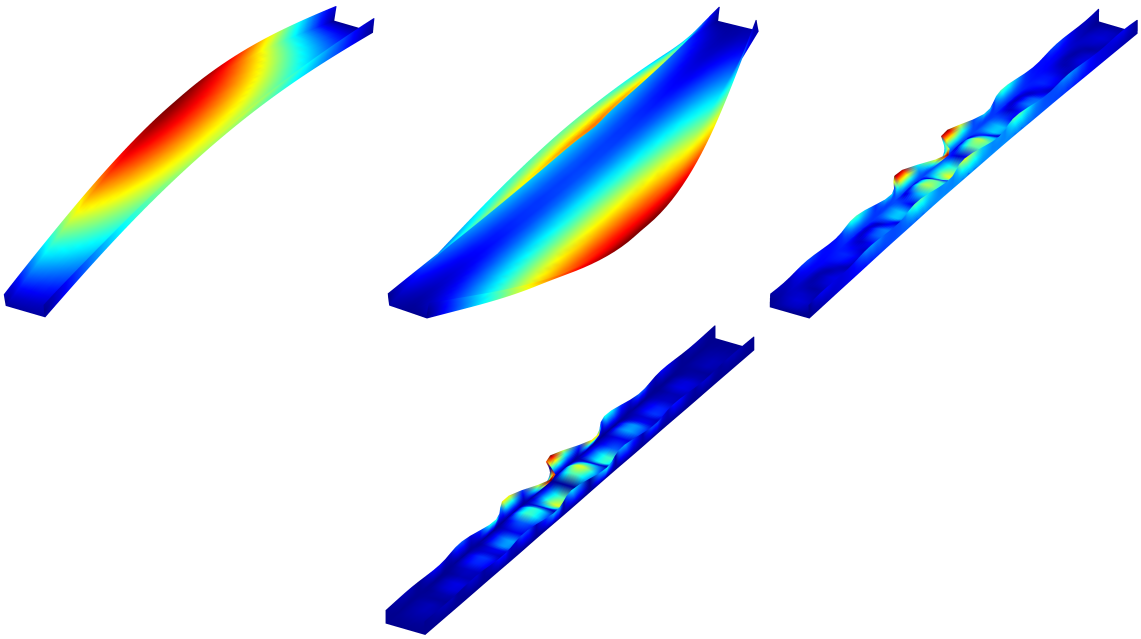

Figure 8: Channel section: Buckling modes

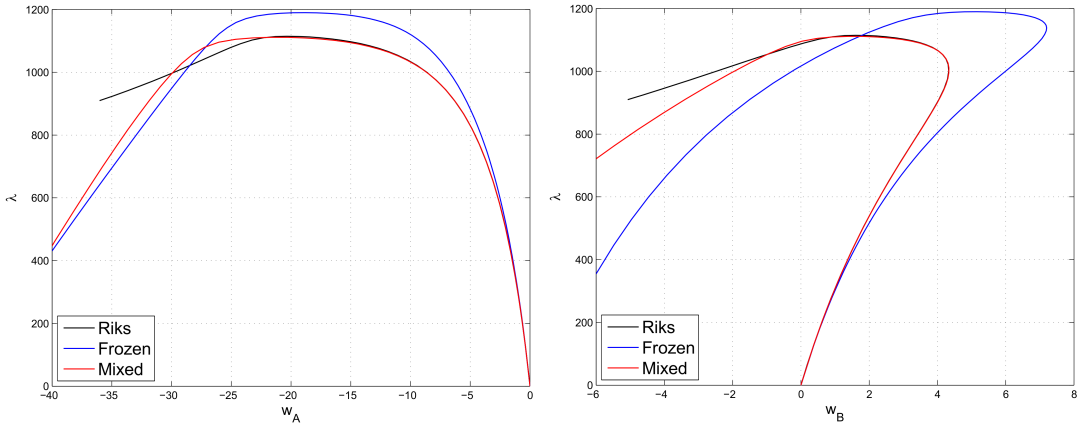

Figure 9: Channel section: Equilibrium paths $\lambda - w_A$, $\lambda - w_B$

	Mixed	Compatible	Mixed MN
steps	24	74	45
loops	73	175	233

Table 4: Channel section: steps and iterations for path–following analysis.

The strong effect of modal interaction between the third (local) mode and the first two flexural–torsional (global) modes is shown.

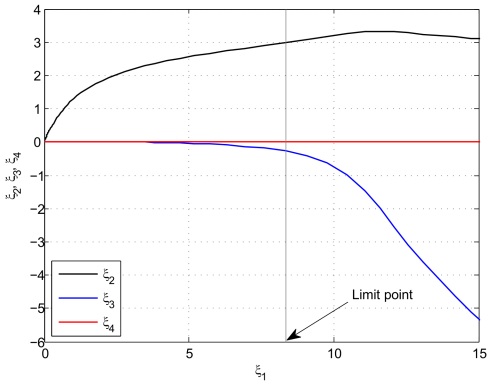

Figure 10: Channel section: Equilibrium paths in ξ_k space.

The results of the mixed asymptotic analysis are in good agreement with the path-following ones. In Tab.4 the steps and iterations of the mixed and compatible descriptions are compared. Obviously the equilibrium path is exactly the same but the better performances of the mixed description are evident even when a modified Newton-Raphson method (MN) is adopted.

4.2 A T beam

The second test regards the beam with data reported in Fig. 11. It consists in a simply supported beam with a T shaped section loaded by a shear force acting at the mid-span and by a small imperfection ($\epsilon = 1/1000$) load as reported in the same figure. The precritical behavior exhibits a strong nonlinearity and coupled bucklings are also present in this case. A mesh of $(9 + 9 + 18) \times 100$ elements has been used.

In Fig.12 the first 4 buckling modes, considered in the multimodal Koiter analysis, are plotted.

In Fig.13 the equilibrium paths recovered by using both asymptotic and path-following analysis are reported and compared. The solution is accurately recovered by the asymptotic strategy up to quite large displacements and the occurrence of a secondary bifurcation.

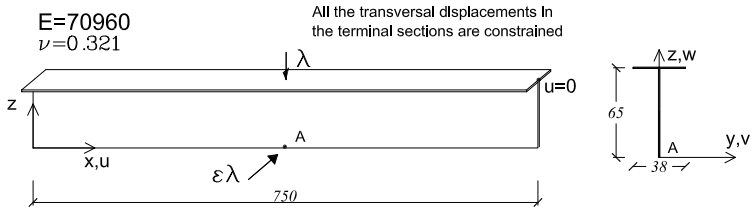

Figure 11: T section beam: geometry and loads

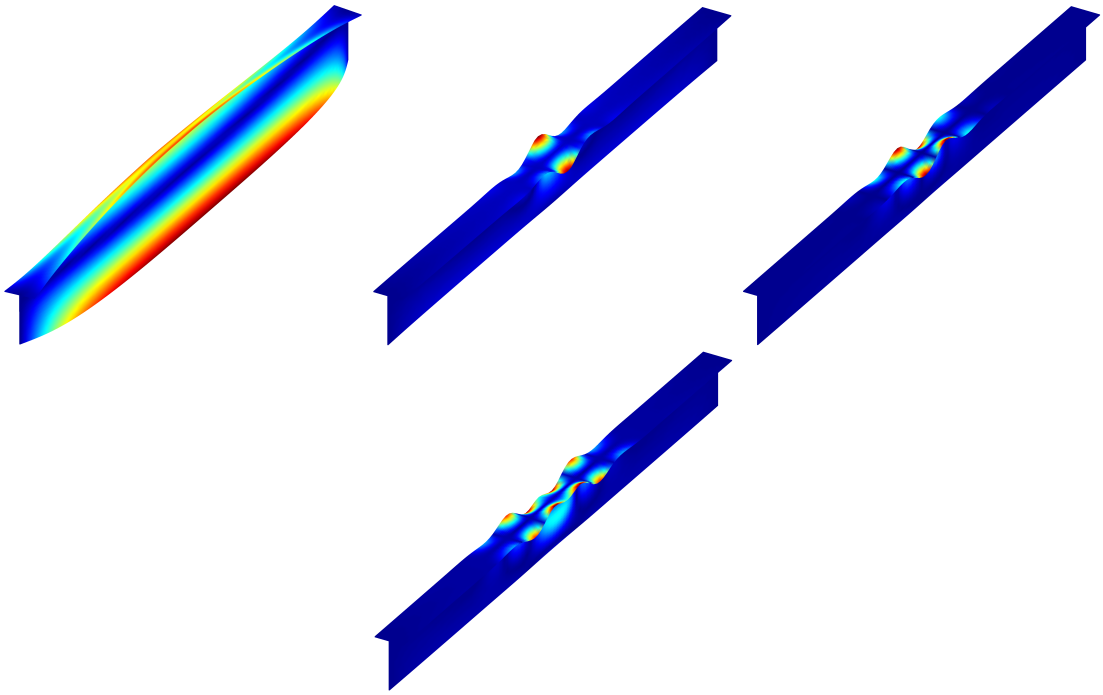

Figure 12: Channel section: First 4 Buckling modes

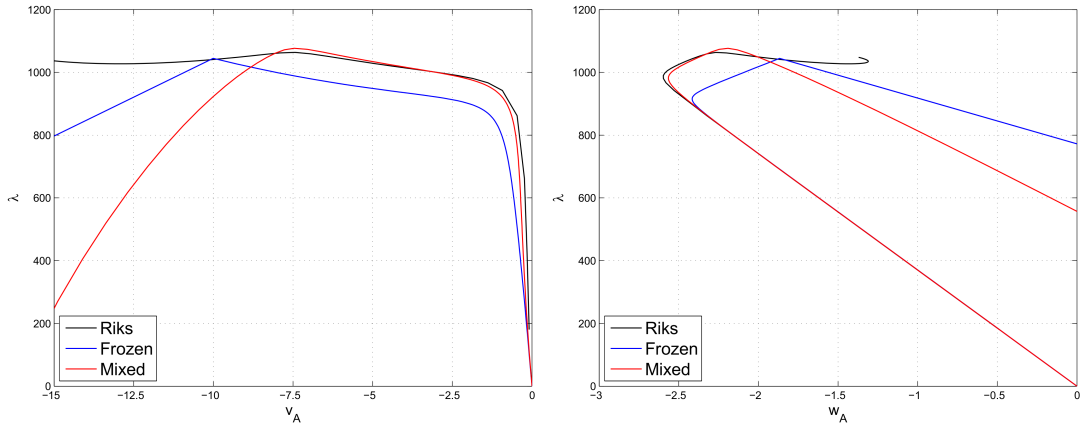

Figure 13: T section beam: Equilibrium paths $\lambda - w_A$, $\lambda - v_A$

	Mixed	Frozen
λ_1	1092.1	936.8
λ_2	1869.1	1860.4
λ_3	1993.5	1989.6
λ_4	2258.9	2252.1

Table 5: T section beam: first 4 buckling loads.

	Mixed	Compatible	Mixed MN
steps	20	42	55
loops	60	169	252

Table 6: T section beam: steps and iterations for path–following analysis.

Also in this case (see Fig.14) the equilibrium path is plotted in terms of the modes amplitudes ξ_k showing a strong interaction among modes 1, 2 and 4.

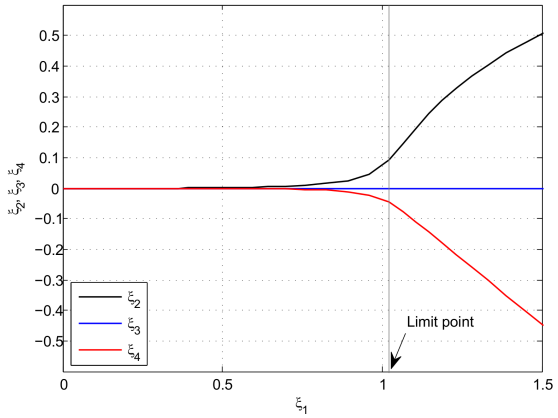

Figure 14: T section beam: Equilibrium paths in ξ_k space.

In Tab.6 the steps and iterations of the mixed, using both full o modified Newton (MN) methods, and compatible descriptions are compared. This example highlights the excellent performances of the mixed description even more than the previous test.

4.3 A simple frame

Finally Fig. 15 reports the geometry and the material properties of a simple portal frame, similar to that analyzed in [52]. It consists of two beams with a C shaped section loaded as depicted in the same figure. Coupled instability is present also in this case. Both the beams are discretized using a mesh of $(6+12+6)\times 40$ elements. The node discretization is automatically defined from those of the two beams.

In Fig.16 the first 3 buckling modes considered in the multimodal Koiter analysis are reported.

Also in this case the equilibrium paths recovered using both the asymptotic and path-following analysis are reported and compared in Fig.17. The frozen configuration asymptotic analysis furnishes a similar equilibrium path to the mixed one but an overestimate in the limit load. The mixed Koiter analysis accurately recovers the solution up to quite large displacements.

In Fig.18 the equilibrium path is plotted in terms of the modes amplitudes ξ_k showing a

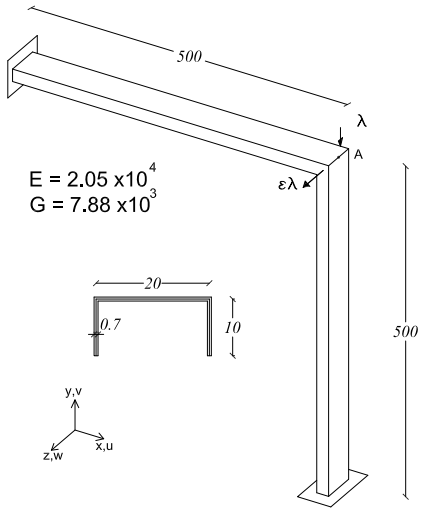

Figure 15: T section beam

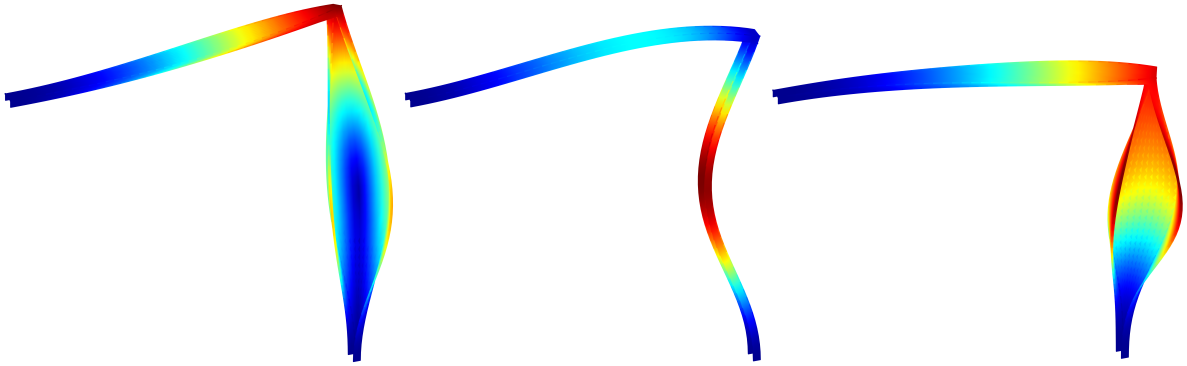

Figure 16: Simple frame: First 3 Buckling modes

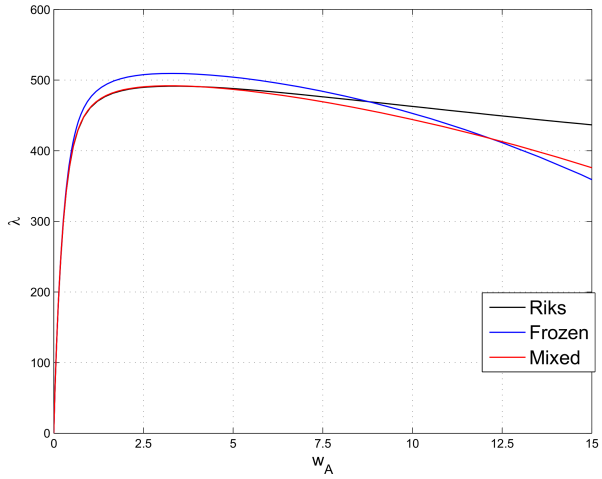

Figure 17: Simple frame: Equilibrium paths $\lambda - w_A$

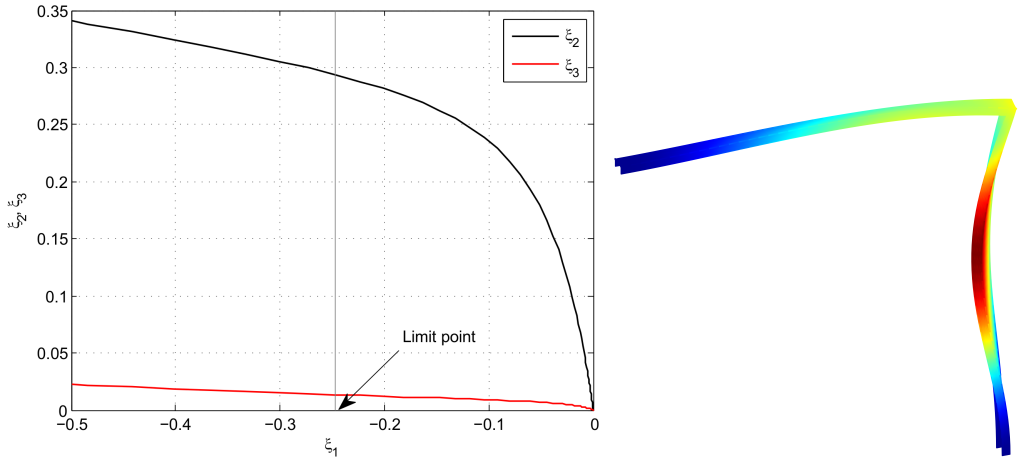

Figure 18: Simple frame: deformed shape at the limit point and equilibrium paths in ξ_k space

	Mixed	Frozen
λ_1	588.92	641.01
λ_2	683.50	684.59
λ_3	1025.90	993.66

Table 7: Simple frame: first 3 buckling loads.

strong interaction among modes 1, 2. In the same figure the deformed configuration at the limit point is also reported.

Finally in Tab.8 the steps and iterations required by the mixed, using full and modified Newton method, and compatible descriptions are compared.

5 Conclusions

In this paper the better performances of mixed elements in the nonlinear analysis of slender structures have been shown and explained. To focus on the origin of this behavior, which is independent of the finite element interpolation, a compatible description of a mixed 3D solid finite element has been derived. In this way it has been possible to show how the compatible description, and so any compatible finite element, is affected by an underhand and neglected extrapolation locking phenomenon that produces slow or lack of convergence for the path–following analyses and inaccurate solutions for the Koiter method. The occurence of the locking has been theoretically investigated and it has been indicated that it is due to the presence of directions with different stiffness as typically occurs for slender structures which are usually characterized by a high membranal/flexural stiffness ratio. These conclusions are general and hold for any nonlinear structural model and finite element.

Many advantages of solid elements in geometrically nonlinear analysis are already known in literature. In this paper we show further important properties of mixed solid FE within the Koiter asymptotic formulation. In fact, due to the simple 3rd order dependence of the strain energy on

	Mixed	Compatible	Mixed MN
steps	24	51	51
loops	73	196	198

Table 8: Simple Frame: steps and iterations for path–following analysis.

its FE parameters, all the higher order energy variations are null and so it is possible to have: i) an exact linear bifurcation analysis with improvements in its computational efficiency and accuracy for non near buckling loads; ii) simplification and greater accuracy in the evaluation of the energy variations required to recover the equilibrium path with a gain in terms of the computational cost; iii) a more simple and effective numerical method which is easy to include in FE packages.

REFERENCES

[1] Sze K, Chan W, Pian T. An eight-node hybrid-stress solid-shell element for geometric non-linear analysis of elastic shells. *International Journal for Numerical Methods in Engineering* 2002; **55**(7):853–878.

[2] Klinkel S, Gruttmann F, Wagner W. A robust non-linear solid shell element based on a mixed variational formulation. *Computer Methods in Applied Mechanics and Engineering* 2006; **195**(1-3):179–201.

[3] Vu-Quoc L, Tan XG. Optimal solid shells for non-linear analyses of multilayer composites. I Statics. *Computer Methods in Applied Mechanics and Engineering* 2003; **192**(9-10):975–1016.

[4] Li Q, Liu Y, Zhang Z, Zhong W. A new reduced integration solid-shell element based on EAS and ANS with hourglass stabilization. *International Journal for Numerical Methods in Engineering* 2015; 1885–1891.

[5] Garcea G, Madeo A, Casciaro R. The implicit corotational method and its use in the derivation of nonlinear structural models for beams and plates. *J. Mech. Mater. Struct.* 2012; **7**(6):509–539.

[6] Garcea G, Madeo A, Casciaro R. Nonlinear FEM analysis for beams and plate assemblages based on the implicit corotational method. *J. Mech. Mater. Struct.* 2012; **7**(6):539–574.

[7] Genoese A, Genoese A, Bilotta A, Garcea G. A geometrically exact beam model with non-uniform warping coherently derived from the saint venant rod. *Engineering Structures* 2014; **68**:33–46.

[8] Sze K. Three-dimensional continuum finite element models for plate/shell analysis. *Prog. Struct. Engng. Mater* 2002; **4**:400–407.

[9] Klinkel S, Gruttmann F, Wagner W. Continuum based three-dimensional shell element for laminated structures. *Computers and Structures* 1999; **71**(1):43–62.

[10] Reese S, Wriggers P, Reddy BD. New locking-free brick element technique for large deformation problems in elasticity. *Computers and Structures* 2000; **75**(3):291–304.

[11] Schwarze M, Reese S. A reduced integration solid-shell finite element based on the EAS and the ANS conceptGeometrically linear problems. *Computer Methods in Applied Mechanics and Engineering* 2009; (80):1322–1355.

[12] Schwarze M, Reese S. A reduced integration solid-shell finite element based on EAS and the ANS concept: Large deformation problems. *International Journal for Numerical Methods in Engineering* 2011; (85):289–329.

[13] Sze K, Ghali A. Hybrid hexahedral element for solids, plates, shells and beams by selective scaling. *International Journal for Numerical Methods in Engineering* 1993; **36**(9):1519–1540.

[14] Vu-Quoc L, Tan X. Efficient Hybrid-EAS solid element for accurate stress prediction in thick laminated beams, plates, and shells. *Computer Methods in Applied Mechanics and Engineering* 2013; **253**:337–355.

[15] Frischkorn J, Reese S. A solid-beam finite element and non-linear constitutive modelling. *Computer Methods in Applied Mechanics and Engineering* Oct 2013; **265**:195–212.

[16] Sze K, Liu X, Lo S. Hybrid-stress six-node prismatic elements. *International Journal for Numerical Methods in Engineering* 2004; **61**(9):1451–1470.

[17] Sze K, Zheng SJ. A stabilized hybrid-stress solid element for geometrically nonlinear homogeneous and laminated shell analyses. *Computer Methods in Applied Mechanics and Engineering* 2002; **191**(17-18):1945–1966.

[18] Sze K, Liu X, Lo S. Hybrid-stress six-node prismatic elements. *International Journal for Numerical Methods in Engineering* 2004; **61**(9):1451–1470.

[19] Sze K, Lo S, Yao LQ. Hybrid-stress solid elements for shell structures based upon a modified variational functional. *International Journal for Numerical Methods in Engineering* 2002; **53**(12):2617–2642.

[20] Sze K, Yao L. A hybrid stress ANS solid-shell element and its generalization for smart structure modelling. Part I - solid-shell element formulation. *International Journal for Numerical Methods in Engineering* 2000; **48**(4):545–564.

[21] Wu D, Lo S, Sheng N, Sze K. Universal three-dimensional connection hexahedral elements based on hybrid-stress theory for solid structures. *International Journal for Numerical Methods in Engineering* 2010; **81**(3):307–334.

[22] Sze K, Zheng SJ, Lo S. A stabilized eighteen-node solid element for hyperelastic analysis of shells. *Finite Elements in Analysis and Design* 2004; **40**(3):319–340.

[23] Sze K, Yao LQ, Pian T. An eighteen-node hybrid-stress solid-shell element for homogenous and laminated structures. *Finite Elements in Analysis and Design* 2002; **38**(4):353–374.

[24] Garcea G, Trunfio G, Casciaro R. Mixed formulation and locking in path-following nonlinear analysis. *Computer Methods in Applied Mechanics and Engineering* NOV 2 1998; **165**(1-4):247–272.

[25] Garcea G, Salerno G, Casciaro R. Extrapolation locking and its sanitization in Koiter's asymptotic analysis. *Computer Methods in Applied Mechanics and Engineering* 1999; **180**(1-2):137–167.

[26] Garcea G, Madeo A, Zagari G, Casciaro R. Asymptotic post-buckling FEM analysis using corotational formulation. *International Journal of Solids and Structures* 2009; **46**(2):377–397.

[27] Garcea G, Trunfio GA, Casciaro R. Path-following analysis of thin-walled structures and comparison with asymptotic post-critical solutions. *International Journal for Numerical Methods in Engineering* 2002; **55**(1):73–100.

[28] Garcea G, Bilotta A, Madeo A, Casciaro R. *Direct evaluation of the post-buckling behavior of slender structures through a numerical asymptotic formulation*. Springer Verlag, 2014.

[29] Casciaro R. Computational Asymptotic Post-Buckling Analysis of Slender Elastic Structures. *CISM Courses and Lectures NO. 470* 2005; :.

[30] Riks E. An incremental approach to the solution of snapping and buckling problems. *International Journal of Solids and Structures* 1979; **15**(7):529–551.

[31] Lacarbonara W. *Nonlinear Structural Mechanics*. Spinger Verlag: New-York, 2013.

[32] Lanzo AD, Garcea G, Casciaro R. Asymptotic post-buckling analysis of rectangular plates by hc finite elements. *International Journal for Numerical Methods in Engineering* 1995; **38**(14):2325–2345.

[33] Lanzo AD, Garcea G. Koiter's analysis of thin-walled structures by a finite element approach. *International Journal for Numerical Methods in Engineering* 1996; **39**(17):3007–3031.

[34] Casciaro R, Garcea G, Attanasio G, Giordano F. Perturbation approach to elastic post-buckling analysis. *Computers & Structures* 1998; **66**(5):585–595.

[35] Garcea G. Mixed formulation in Koiter analysis of thin-walled beams. *Computer Methods in Applied Mechanics and Engineering* 2001; **190**(26-27):3369–3399.

[36] Dubina D, Ungureanu V. Instability mode interaction: From van der neut model to ecbl approach. *Thin-Walled Structures* 2014; **81**:39–49.

[37] Rahman T, Jansen E. Finite element based coupled mode initial post-buckling analysis of a composite cylindrical shell. *Thin-Walled Structures* 2010; **48**(1):25–32.

[38] Flores F, Godoy L. Elastic post-buckling analysis via finite element and perturbation techniques. part 1: Formulation. *International Journal for Numerical Methods in Engineering* 1992; **33**(9):1775–1794.

[39] Barbero E, Raftoyiannis I, Godoy L. Finite elements for post-buckling analysis. ii-application to composite plate assemblies. *Computers and Structures* 1995; **56**(6):1019–1028.

[40] Boutyour E, Zahrouni H, Potier-Ferry M, Boudi M. Asymptotic-numerical method for buckling analysis of shell structures with large rotations. *Journal of Computational and Applied Mathematics* 2004; **168**(1-2):77–85.

[41] Silvestre N, Camotim D. Asymptotic-numerical method to analyze the postbuckling behavior, imperfection-sensitivity, and mode interaction in frames. *Journal of Engineering Mechanics* 2005; **131**(6):617–632.

[42] Schafer B, Graham-Brady L. Stochastic post-buckling of frames using koiter's method. *International Journal of Structural Stability and Dynamics* 2006; **6**(3):333–358.

[43] Chen H, Virgin L. Finite element analysis of post-buckling dynamics in plates-part i: An asymptotic approach. *International Journal of Solids and Structures* 2006; **43**(13):3983–4007.

[44] Rizzi NL, Varano V, Gabriele S. Initial postbuckling behavior of thin-walled frames under mode interaction. *Thin-Walled Structures* 2013; **68**:124 – 134.

[45] White S, Raju G, Weaver P. Initial post-buckling of variable-stiffness curved panels. *Journal of the Mechanics and Physics of Solids* 2014; **71**(1):132–155.

[46] Koiter W. On the stability of elastic equilibrium.

[47] Barbero E, Madeo A, Zagari G, Zinno R, Zucco G. Imperfection sensitivity analysis of laminated folded plates. *Thin-Walled Structures* 2015; **90**:128 – 139.

[48] Liang K, Ruess M, Abdalla M. The Koiter-Newton approach using von Karman kinematics for buckling analyses of imperfection sensitive structures. *Computer Methods in Applied Mechanics and Engineering* 2014; **279**:440–468.

[49] Liang K, Abdalla M, Grdal Z. A Koiter-Newton approach for nonlinear structural analysis. *International Journal for Numerical Methods in Engineering* 2013; **96**(12):763–786.

[50] Pian THH, Wu CC. *Hybrid and Incompatible Finite Element Methods*. Chapman & All, CRC: New-York, 1969.

[51] Zagari G, Madeo A, Casciaro R, De Miranda S, Ubertini F. Koiter analysis of folded structures using a corotational approach. *International Journal of Solids and Structures* 2013; **50**(5):755–765.

[52] Genoese A, Genoese A, Bilotta A, Garcea G. Buckling analysis through a generalized beam model including section distortions. *Thin-Walled Structures* 2014; **85**:125–141.